(Online First) Synthesis, Structural, Thermal and Luminescence Studies of new DABCO bismuthate (III) hybrid material

Marwen Chouri & Habib Boughzala*

Laboratoire de Matériaux et Cristallochimie, Faculté des Sciences de Tunis, Université de Tunis El Manar, 2092 Tunis, Tunisia.*
email : habib.boughzala@ipein.rnu.tn

Abstract: The title compound Bis(1,4-diazabicyclo[2.2.2]octane)octachlorido-di-bismuthate (III) dihydrate was obtained by slow evaporation at room temperature of a hydrochloric aqueous solution (pH=1) containing bismuth (III) nitrate and the 1,4-diazabicyclo[2.2.2]octane (DABCO) in a 1:2 molar ratio. This material crystallizes in the $P2_1/c$ monoclinic space group with a=7.875(1)Å, b=18.380(2)Å, c=10.445(2)Å, β=105.95(1)° and Z=2.

The structure exhibits a zero-dimensional (0D) periodic arrangement of bioctahedra $(Bi_2Cl_{10})^{4-}$ surrounded by organic cations 1,4-diazabicyclo[2.2.2]octane (DABCO). The crystal cohesion is achieved by N-H…Cl, N-H…O and O-H…Cl hydrogen interaction linking the different parts of the structure. This compound was characterized by different techniques such as IR, DSC, TGA-DTA, XRD, XPRD and photoluminescence (PL) at room temperature.

Keywords: Hybrid, 0-D arrangement, gap energy, semi-conductor, Crystal Structure, Powder Diffraction.

1. Introduction

In recent years, many researches on organic-inorganic hybrid compounds were made thanks to their sighted interesting physical behavior and applications in optoelectronics[1]. The main interesting optical activity observed in this kind of compounds is generally the result of the presence of an active lone pair $ns^{2[2]}$ in the inorganic clusters or a drastic distortion in the organic cations[3-4] or a combination of the properties of the two moieties. In particular for the halogenated bismuth or antimony anionic networks[5-6] the anionic arrangement leads to 4 kinds of dimensionalities: the quantum dots (0D) observed in hybrids such as $(C_6H_{14}N_2)_2[Sb_2Cl_{10}]2H_2O^{[7]}$, the quantum wire (1D) as it's the case of $(C_2H_7N_4O)_{2[}BiCl_5]^{[8]}$, quantum well (2 D) or bi-dimensional class and the bulk (3D) topology. The organic cations are filling the empty space left by the inorganic network.

In this work, synthesis, X-ray diffraction, crystal structure and optical behavior investigation of a new 0-D hybrid compound based on bismuth $(C_6H_{14}N_2)_2[Bi_2Cl_{10}].2H_2O$ are presented.

2. Experimental

2.1 Synthesis

Under ambient conditions the $(C_6H_{14}N_2)_2[Bi_2Cl_{10}].2H_2O$ crystals were obtained by dissolving $Bi(NO_3)_3.5H_2O$ and DABCO $(C_6H_{12}N_2)$ in water in a 1:2 molar ratio. The pH of the solution was adjusted to 1. The mixture was stirred and kept for several days. Bulks like colorless crystals were obtained few weeks later.

2.2 X-ray data collection

The single crystal diffraction measurements were performed at room temperature on an Enraf-Nonius CAD-4[9]

four circle diffractometer using MoK$_\alpha$ radiation (λ=0.71073 Å). The bismuth heavy atoms and chlorine were located from a three-dimensional Patterson map using SHELXS-97[11]. All non-hydrogen atoms positions were found using successive difference Fourier Maps. The structure was refined by full-matrix last square by SHELXL-97 using anisotropic thermal parameters. Hydrogen atoms were positioned geometrically using appropriate SHELXL-97 command for water molecule for both carbon and nitrogen atoms. The refinement was carried out using WinGX 1.80.05[12] package. Table 1 resumes the crystal data, the single crystal diffraction conditions and the refinement parameters. The Table 2 summarizes the refined atomic parameters. The complete set of the structural parameters in CIF format is available from the Cambridge Crystallographic Database Centre (CCDC 971956). A copy can be obtained free of charge from www.ccdc.cam.ac.uk/data_request/cif or deposit@ccdc.edu.

The powder diffraction pattern was obtained by a D8 ADVANCE Bruker diffractometer with a Lynxeye accelerator using Cu (Kα$_1$/α$_2$ =1.54060/1.54439 Å) wavelength with step-scanning (Δ2θ = 0.02°) constant time interval of 0.1 s.

Table 1: Crystal data and structure refinement for $(C_6H_{14}N_2)_2[Bi_2Cl_{10}].2H_2O$ compound.

Chemical formula	$Bi_2Cl_{10}\cdot2(C_6H_{14}N_2)\cdot2(H_2O)$
Empirical formula	$Bi_2Cl_{10}\,C_{12}\,H_{32}\,N_4\,O_2$
Formula weight	1036.88 g.mol^{-1}
Temperature	293(2) K
Crystal system	Monoclinic
Space group	P 2$_1$/c
a (Å)	7.875(3)
b (Å)	18.379(5) Å
c (Å)	10.444(4) Å
β (°)	105.95(3) °
V (Å^3)	1453.4(9)
Z	2
Absorption coefficient (mm^{-1})	13.027
Calculated density	2.369 g.cm^{-3}
Crystal size	0.15 x 0.29 x 0.43 (mm)^3
Crystal habit	colorless prism
Data collection	
Diffractometer	Enraf-Nonius CAD4

Monochromator	graphite
Radiation type, Wavelength	Mo(K), 0.071073
q range for data collection	2.22 - 26.97 °
Indexes range	$-10 \leq h \leq 1$, $-1 \leq k \leq 23$, $-12 \leq l \leq 13$
Absorption correction	psi-scan
T_{max}/T_{min}	0.013,0.074
Collected reflections	3159
Independent reflections	3159
Observed reflections	$2681[I > 2\sigma(I)]$
R_{int}	0.035
Refinement	
Refinement method	Full-matrix last square on F^2
$R[F^2 > 2\sigma(F^2)]$	0.036
wR (F^2)	0.102
R_{int}	0.035
$(\sin q/\lambda)_{max}$ (Å^{-1})	0.638
Goodness-of-fit on F^2	S=1.06
Dr_{min} / Dr_{max}	-2.57 e Å^{-3} / 3.48 e Å^{-3}

Table 2: Fractional atomic coordinates and isotropic displacement parameters (Å^2).

Atom	x	y	z	Uiso*/Ueq
Bi	0.42097 (3)	0.42073 (2)	0.34670 (2)	0.02518 (11)
Cl1	0.2576 (2)	0.50934 (10)	0.50438 (18)	0.0329 (4)
Cl2	0.4635 (3)	0.32483 (10)	0.54389 (18)	0.0361 (4)
Cl3	0.1117 (3)	0.36755 (11)	0.2279 (2)	0.0441 (5)
Cl4	0.3821 (3)	0.52442 (12)	0.1571 (2)	0.0438 (5)
Cl5	0.5941 (4)	0.33648 (14)	0.2288 (3)	0.0635 (7)
Ow	0.7852 (9)	0.2151 (4)	0.4798 (8)	0.0609 (18)
Hw1	0.701 (11)	0.194 (6)	0.501 (12)	0.070*
Hw2	0.732 (14)	0.251 (4)	0.434 (10)	0.070*

N1	0.0157 (8)	0.3538 (3)	0.8660 (6)	0.0291 (12)
H1	−0.0668	0.3405	0.9173	0.035*
N2	0.2250 (8)	0.3886 (3)	0.7369 (6)	0.0319 (13)
H2	0.3082	0.4026	0.6866	0.038*
C1	0.1780 (10)	0.3089 (4)	0.9111 (8)	0.0340 (16)
H1A	0.1513	0.2584	0.8867	0.041*
H1B	0.2238	0.3117	1.0072	0.041*
C6	0.0703 (11)	0.3511 (5)	0.6456 (7)	0.0403 (19)
H6A	0.1062	0.3045	0.6179	0.048*
H6B	0.0224	0.3805	0.5668	0.048*
C3	0.0613 (10)	0.4331 (4)	0.8868 (8)	0.0344 (16)
H3A	−0.0457	0.4618	0.8708	0.041*
H3B	0.1310	0.4413	0.9778	0.041*
C4	0.1641 (11)	0.4551 (4)	0.7924 (8)	0.0385 (17)
H4A	0.0904	0.4841	0.7209	0.046*
H4B	0.2650	0.4843	0.8386	0.046*
C5	−0.0695 (11)	0.3398 (5)	0.7206 (7)	0.0386 (17)
H5A	−0.1673	0.3731	0.6874	0.046*
H5B	−0.1147	0.2905	0.7078	0.046*
C2	0.3144 (11)	0.3374 (4)	0.8454 (8)	0.0385 (17)
H2A	0.4078	0.3625	0.9105	0.046*

Table 3: Selected bond lengths (Å) and angles ( ) for $(C_6H_{14}N_2)_2[Bi_2Cl_{10}].2H_2O$.

Bond	Distance (Å)	Bond	Angle (°)	Bond	Angle (°)
Bi—Cl5	2.588 (2)	Cl5—Bi—Cl3	95.45 (9)	C1—N1—C3	110.1 (6)
Bi—Cl3	2.601 (2)	Cl5—Bi—Cl2	90.07 (8)	C1—N1—C5	109.4 (6)
Bi—Cl2	2.6611 (19)	Cl3—Bi—Cl2	91.28 (7)	C3—N1—C5	109.6 (6)
Bi—Cl4	2.704 (2)	Cl5—Bi—Cl4	92.39 (9)	C4—N2—C2	110.9 (6)
Bi—Cl1	2.8611 (19)	Cl3—Bi—Cl4	90.73 (7)	C4—N2—C6	109.6 (6)
Bi—Cl1[i]	2.884 (2)	Cl2—Bi—Cl4	176.65 (6)	C2—N2—C6	109.0 (6)
Cl1—Bi[i]	2.884 (2)	Cl5—Bi—Cl1	173.58 (8)	N1—C1—C2	108.5 (6)
N1—C1	1.485 (9)	Cl3—Bi—Cl1	88.74 (7)	N2—C6—C5	108.0 (6)
N1—C3	1.503 (9)	Cl2—Bi—Cl1	84.97 (6)	C4—C3—N1	108.5 (6)
N1—C5	1.503 (9)	Cl4—Bi—Cl1	92.40 (7)	N2—C4—C3	109.0 (6)
N2—C4	1.488 (10)	Cl5—Bi—Cl1[i]	91.38 (8)	N1—C5—C6	108.0 (6)
N2—C2	1.492 (9)	Cl3—Bi—Cl1[i]	173.16 (6)	N2—C2—C1	108.4 (6)
N2—C6	1.494 (10)	Cl2—Bi—Cl1[i]	88.44 (6)		
C1—C2	1.517 (11)	Cl4—Bi—Cl1[i]	89.25 (6)		
C6—C5	1.531 (11)	Cl1—Bi—Cl1[i]	84.43 (6)		
C3—C4	1.493 (11)	Bi—Cl1—Bi[i]	95.57 (6)		
Symmetry code: (i) −x+1, −y+1, −z+1.					

Table 4: Hydrogen bond lengths (Å) and angles ( ) for $(C_6H_{14}N_2)_2[Bi_2Cl_{10}].2H_2O$.

D—H···A	D—H	H···A	D···A	D—H···A
Ow—Hw2···Cl5	0.91	2.63	3.458 (8)	163
N1[i]-H1[i]…Ow	0.91	1.87	2.738 (10)	159
Ow—Hw1···Cl5[ii]	0.91	2.80	3.475 (9)	137
N2—H2···Cl1	0.91	2.73	3.351 (7)	127
N2—H2···Cl2	0.91	2.65	3.323 (7)	132
Symmetry codes: (i): 1+x, 0.5-y, -0.5+z) ; (ii): x, 0.5-y, 0.5+z				

2.3 Spectroscopic study, simulated spectra and thermal analysis:

The infrared (IR) investigation was performed on a VERTEX 80/80v FT-IR spectrometer in the spectral domain of 400 – 4000 cm^{-1}. 300 mg of KBr to 3 mg of the compound to prepare the pellet used to produce the IR spectrum.

The photoluminescence spectrum was recorded at room temperature using a HORBIAJOKIN-YVON (HR320) spectrometer equipped with the 488nm line of argon LASER. The compound was dissolved in water and deposed on quartz support.

The calculated IR spectrum was generated using CACHe software[13]. The crystal morphology simulation was carried out using MERCURY software[14]. DSC and TGA-DTA analysis were performed using the DSC 131 EVO in the temperature range of -50 to 250°C.

3. Results

3.1 Structural study

The structural inorganic part of the title compound is made of a couple of chlorinated bismuth $(Bi_2Cl_{10})^{4-}$ sharing one edge. The organic moiety contains two doubly protonated 1,4-Diazabicyclo[2.2.2]octane (DABCO). Two water molecules are involved in the structural unit represented in Figure 1. The different parts are linked by strong hydrogen interactions.

The isolated bi-octahedra $(Bi_2Cl_{10})^{4-}$ are located on an inversion center 2/m leaving around an empty space where the $(DABCOH_2)^{2+}$ moieties are lodged establishing strongly hydrogen interaction with the dimeric deca-chloro-bismuthate (III) $(Bi_2Cl_{10})^{4-}$ by means of N2—H2···Cl2 and N2—H2···Cl1 from both sides. The water molecules are linking the organic and the inorganic moieties via N1—H1···Ow, Ow—Hw2…Cl5 and Ow—Hw1…Cl5 hydrogen bonds as shown on Figure 2. They are playing an important role in the stability and the structural cohesion. The global crystal arrangement can be described by an alternate stacking of organic and inorganic sheets perpendicular to (010) direction and linked by water molecules leading to a three dimensional network visible on Figure 3. Table 3 summarizes the most important geometrical values computed in this structure.

The bonds lengths of bismuth and bridging chlorines (2.863(4) Å and 2.884(4) Å) are longer than terminal ones (2.587(5) Å to 2.704(5) Å). The Cl-Bi-Cl angles vary from 84.46(12)° to 95.4(2)° for cis and 173.25(15)° to 176.64(15)° for trans arrangement proofing the little distortion in the inorganic clusters where the two bismuth are distant of 4.255(2) Å. The observed distortion in the BiCl$_6$ octahedra is probably caused by the bismuth 6s^2 electron pair stereo chemical activity and the hydrogen interaction   Ow—Hw…Cl and N—H…Cl.

The 1.4diazoniabicyclo[2.2.2] octane di-cation bond lengths and angles are normal and comparable to those observed in similar published structures[9]. On the other hand, a visible deviation from the ideal trigonal symmetry of the DABCO molecule can be proofed by the dihedral angles C-N1-N2. Indeed, in the ideal conformation these angles are zero but in our case the average is close to 8.30(5)°.

Playing the role of donor, the water molecule is linked to the $(Bi_2Cl_{10})^{4-}$ by two hydrogen interaction in Ow—Hw1…Cl5^{ii} (ii: 1+x, 0.5-y, -0.5+z) and   Ow—Hw2…Cl5. It is also strongly linked to one organic cation by

N1^i-H1^i…Ow (i: 1+x, 0.5-y, -0.5+z) as an acceptor (see Table 4).

In spite of the low dimensionality (0D) of the anionic network, no noticeable channels, voids or other empty spaces are left by the structural arrangement.
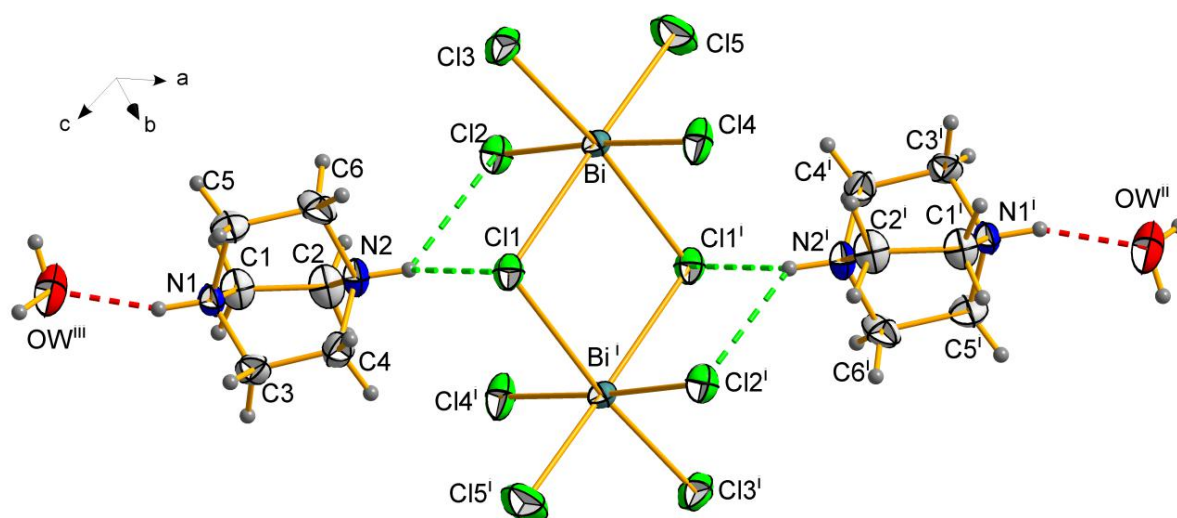
Figure 1: An ORTEP of the structural unit of $(C_6H_{14}N_2)_2[Bi_2Cl_{10}].2H_2O$ showing the molecular sequencing water-organic-inorganic. Carbon's hydrogen was omitted for clarity.

Displacements ellipsoids are drawn with 50% of probability.

[Symmetry code: (i) 1−x, 1−y, 1−z ; (ii) : 2-x, 0.5+y, 0.5-z ; (iii) :-1+x, 0.5-y, 0.5+z]
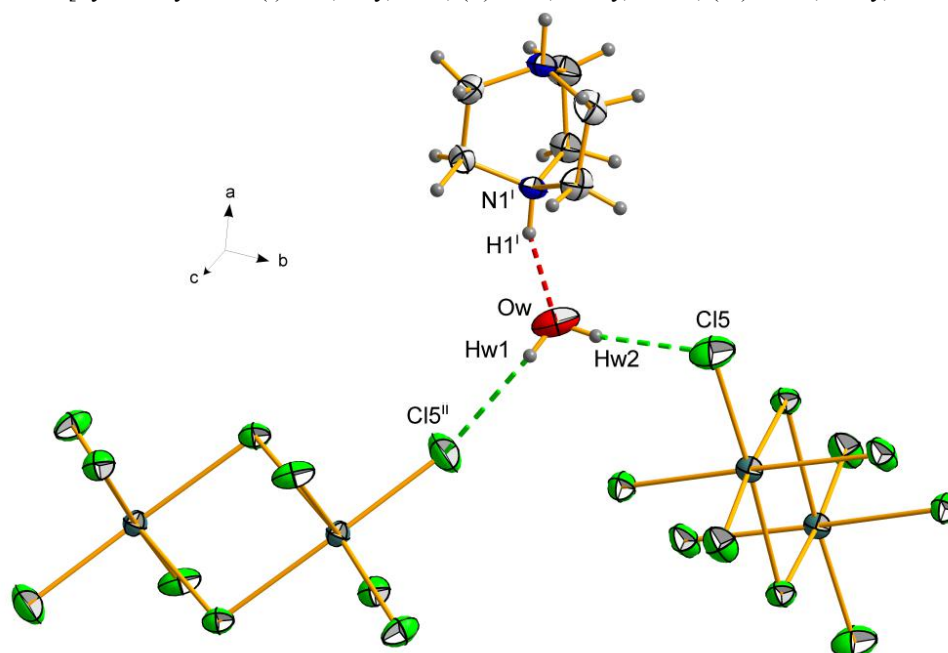
Figure 2: The water molecule linkage in the structure of $(C_6H_{14}N_2)_2[Bi_2Cl_{10}].2H_2O$.

Displacements ellipsoids are drawn with 50% of probability.

[Symmetry code: (i) : 1+x, 0.5-y, -0.5+z ; (ii): x, 0.5-y, 0.5+z]
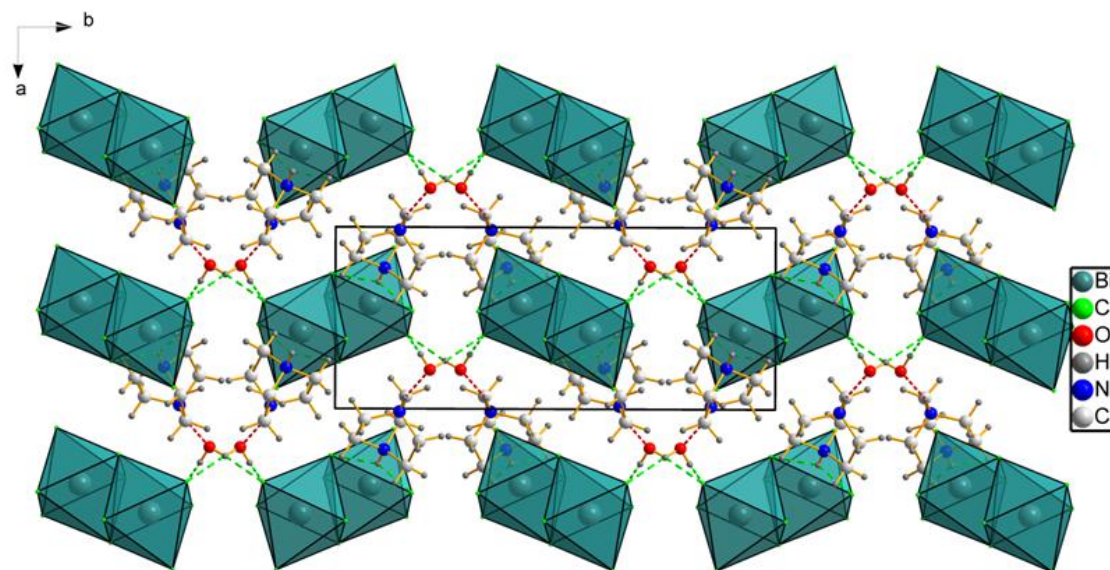
Figure 3: The organic-inorganic alternate stacking layers in the crystal structure of $(C_6H_{14}N_2)_2[Bi_2Cl_{10}].2H_2O$.

3.2 X-ray powder diffraction (XRPD):

It is one of the most powerful characterization techniques in solid state chemistry and materials science. It was used to check the phase purity and the crystallinity of the compound. The absence of amorphous signature and the quality of the observed raw diffraction testify a good crystallinity. Based on the single crystal investigations results, the Rietveld refinement[15] carried out using a slow data collection (figure 4) shows that all the Bragg peaks of the raw diffraction are indexed. Thus, the synthesized powder is endowed with a high purity and the observed physical behavior of the powder can be attributed to the phase $(C_6H_{14}N_2)_2[Bi_2Cl_{10}].2H_2O$.
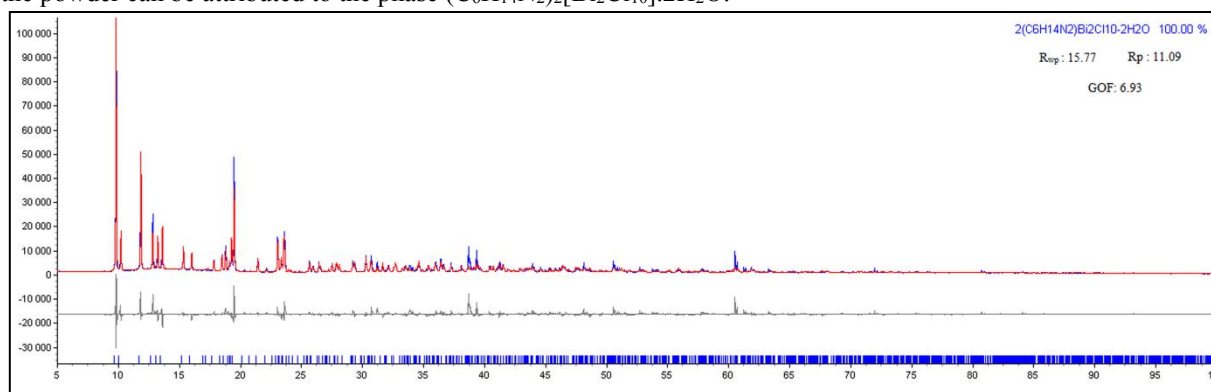
Figure 4: Observed, calculated X-ray diffraction patterns and curve difference for $(C_6H_{14}N_2)_2[Bi_2Cl_{10}].2H_2O$.

3.3 Red-Infrared spectroscopy:

To have more information about the external vibration and deformation modes, the Fast Fourier Transform Infra-Red (FTIR) spectroscopy combined to the semi-empirical Parameterized Model number 3 (PM3) were used to assign the observed frequencies to the vibration modes. The calculated spectra of DABCO and the studied compound are represented respectively in figures 5-a and 5-b and the observed ones in Figure 6. The Table 5 summarizes the observed and the calculated frequencies bands and their correspondent assignments. An important shift is noted between calculated and observed frequencies attributed to the approximations required in the computation algorithms. The main one is to consider isolated molecular units for calculations. Many vibrations and deformations observed in DABCO spectrum can't figure out in the hybrid one such as $\delta_a(NC_3)$, $\delta_s(NC_3)$, $\nu_s(NC_3)$, $\nu_a(C–C)$ and $\gamma_t(CH_2)$. This could be explained by a lack of freedom of the DABCO molecule from both sides thanks to the establishment of new bonds type N-H···Cl and N-H···O[16]. The bands centered around 3490 cm^{-1} for the hybrid material and 3260 cm^{-1} for DABCO

monohydrated confirm the presence of the water molecule.

Table 5: Observed and calculated bands frequencies (cm^{-1}) in the IR spectra of hydrated DABCO and $(C_6H_{14}N_2)_2[Bi_2Cl_{10}].2H_2O$.

Hydrated DABCO		$(C_6H_{14}N_2)_2[Bi_2Cl_{10}].2H_2O.$		Assignment
Calculated	Observed	Calculated	observed	
347	-	-	-	out- γ(C–N–C)
444.5	-	-	488	in-γ(C–N–C)
-	600	-	-	out-δ_a(NC$_3$)
-	660	662.5	-	in-δ_s(NC$_3$)
-	775	-	-	out-δ_s(NC$_3$), out-vs(NC$_3$)
847	841	-	850	in-γr(CH$_2$), δ(C–N–C)
-	910	-	-	va(C–C), in-γt(CH$_2$)
958.3	997			out-δ_s(NC3)
-	1060	-	1060	in-v_a(NC$_3$), v_a(C–C), γt(CH$_2$)
1152.8	-	118.75	-	in-γ_t(CH$_2$)
1208	-	1237.5	1220	-
-	-	-	1280	out-γ_t(CH$_2$)
-	1320	-	1330	in-γ_t(CH$_2$), in-v_a(NC$_3$)
-	-	-	1390	-
-	1460	1425	1450	in-γ_s(CH$_2$)
-	-	-	1610	-
-	1670	-	-	γ_s(O-H)
1736	-	-	-	-
2000-2500	-	-	2000-2500	v(O-H¨Cl)
-	-	2462.5	2610-2880	v(N-H¨Cl)
-	2890	-	3040	out-v_s(CH$_2$)
3000	2960	-	3110	in-v_s(CH$_2$)
3722	3260	-	3490	v_{as}(O-H)
3965	-	3900	-	v_s(O-H)

v – Stretching, δ– bending, γ_s – scissoring, γ_w – wagging, γ_t – twisting, γ_r – rocking, «in» in-phase, «out» out-of-phase.
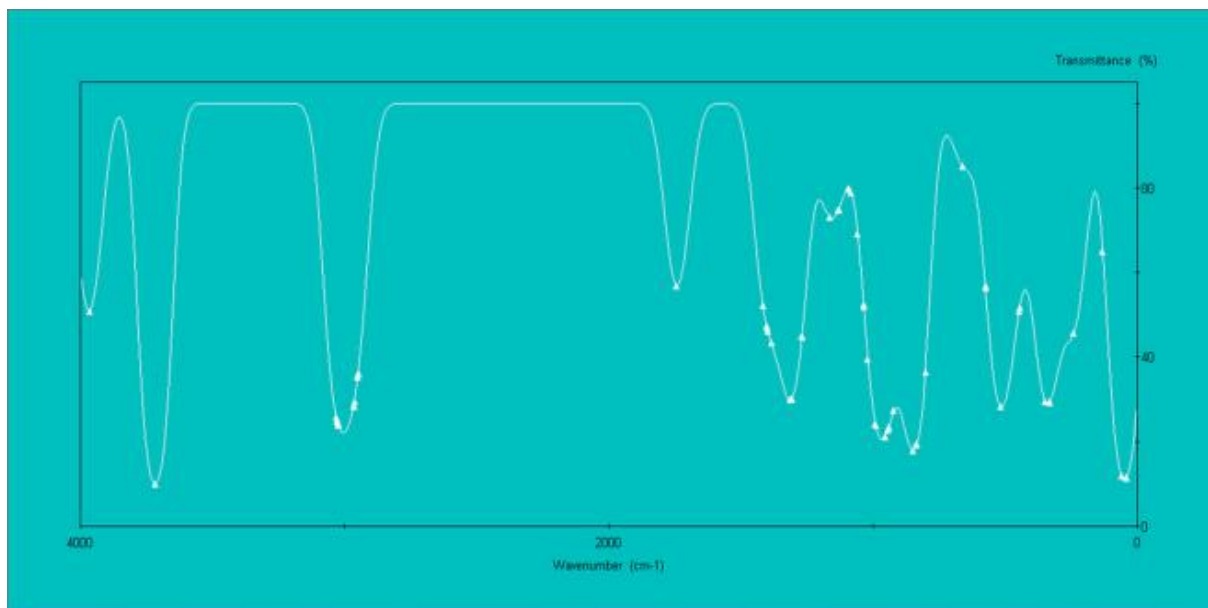
Figure 5-a: The calculated red infrared spectrum of the monohydrated DABCO compound.
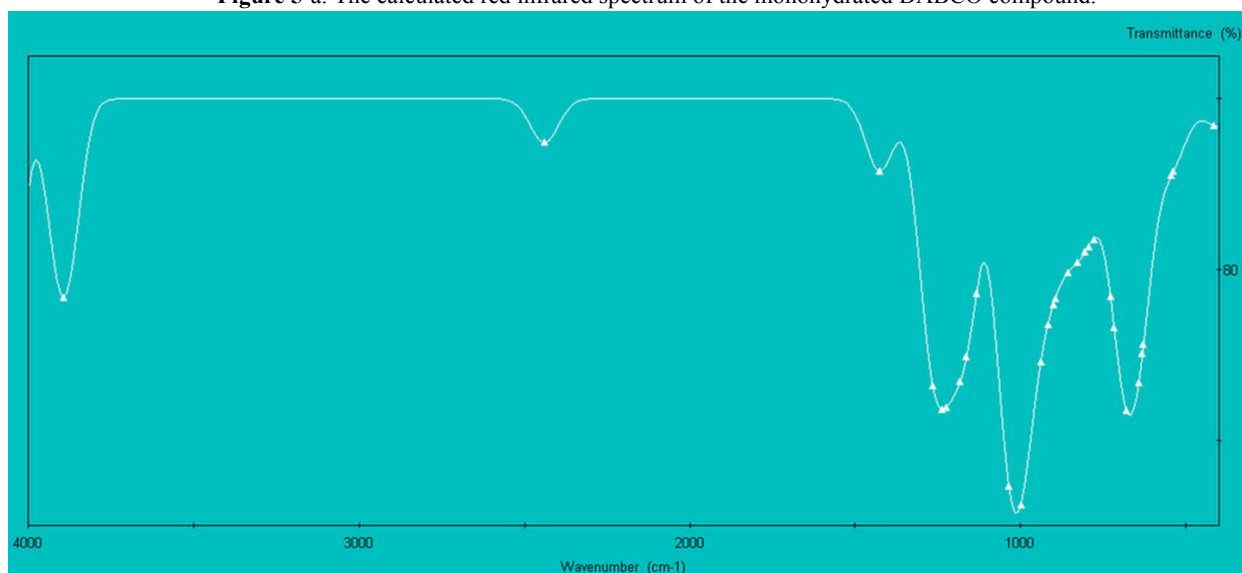
Figure 5-b: The calculated red infrared spectrum of $(C_6H_{14}N_2)_2[Bi_2Cl_{10}].2H_2O$.

3.4 Optical study

The photoluminescence spectrum of the $(C_6H_{14}N_2)_2[Bi_2Cl_{10}].2H_2O$ (Figure 7) exhibits at least three bands located at 1.88, 2.04 and 2.56 eV. Based on the structural study, the High Occupied Molecular Orbital – Low Unoccupied Molecular Orbital (HOMO-LUMO) orbital's energy computation (figure 8-a/8-b) makes easy the assignment of the observed transitions. Furthermore, these results allow the assignment of the compound parts (organic, inorganic or both moieties) to the observed optical phenomenon. The DFT's calculations were carried out by the program CAChe using the semi-empirical Parameterized Model number 3 (PM3) for DABCO monohydrated materials and for the hybrid compound. The difference of energy between HOMO and LUMO orbitals for DABCO monohydrated is 11.363 eV and 1.929 eV for $(C_6H_{14}N_2)_2[Bi_2Cl_{10}].2H_2O$ where the HOMO is located on the inorganic part and the LUMO is on the organic moiety. Thus, in this case, both parts of the hybrid structure are actors of the observed luminescence behavior. Accordingly to the first observed band gap value (1.88 eV) in the photoluminescence spectrum and its homologous in the calculated one (1.93 eV), the title compound can be considered as a semi-conductor material. The second observed band centered on 2.04 eV can be another energy gap but did not appear in the HOMO-LUMO calculation

explained by a transition for a higher level of energy (figure 9). The third band centered at 2.56(3) eV is probably due to the exciton emission ($E_{exciton}$= 2.54 eV) which is the energy of the argon ion LASER.
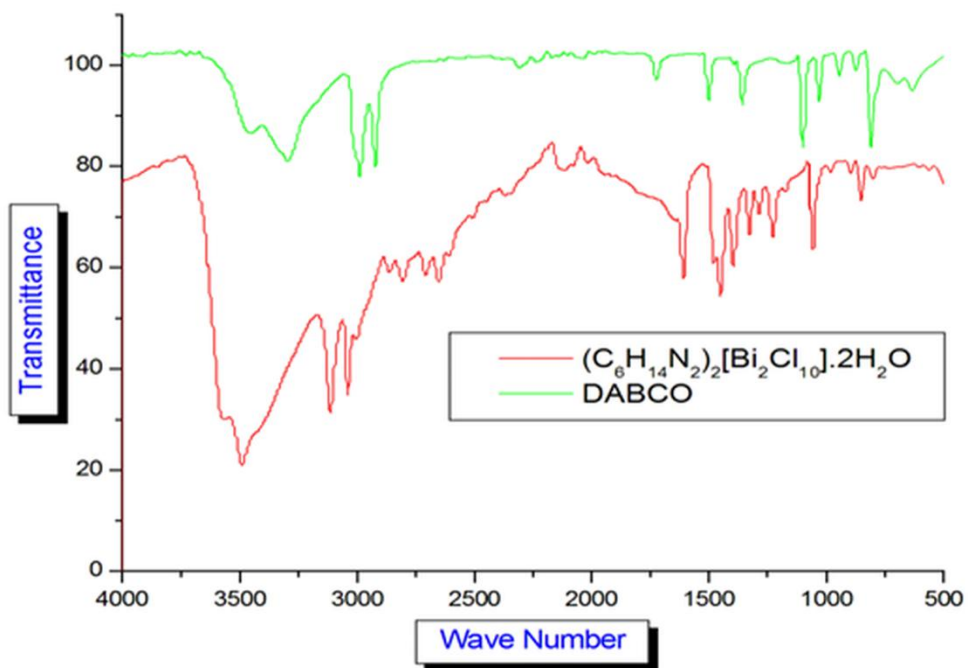
Figure 6: FTIR spectrums of the organic DABCO and hybrid compound.
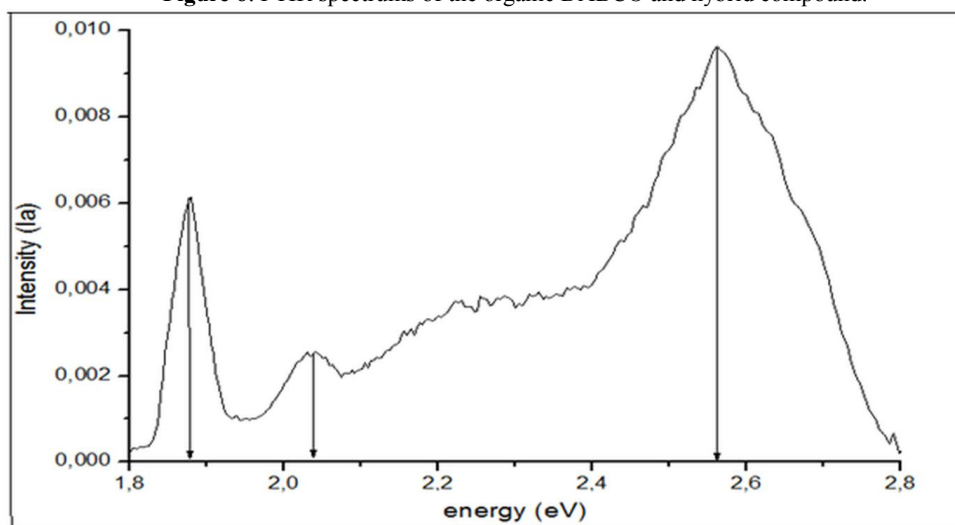
Figure 7: Luminescence spectrum relative to hybrid films.
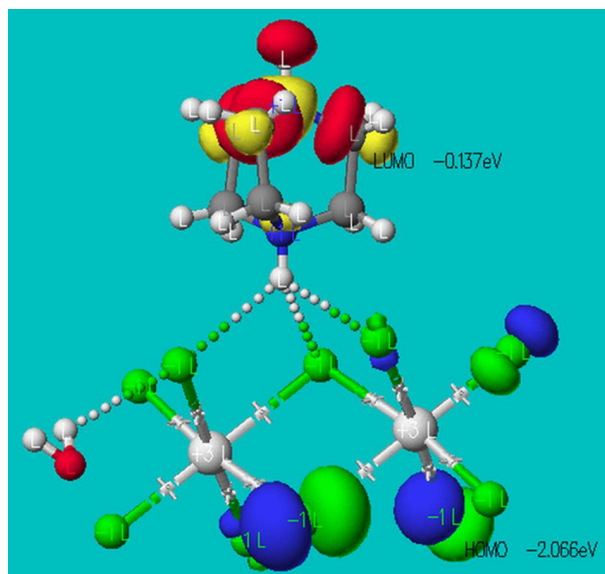
Figure 8-a: Calculated energy of HOMO-LUMO orbital of the $(C_6H_{14}N_2)_2[Bi_2Cl_{10}].2H_2O$ material.
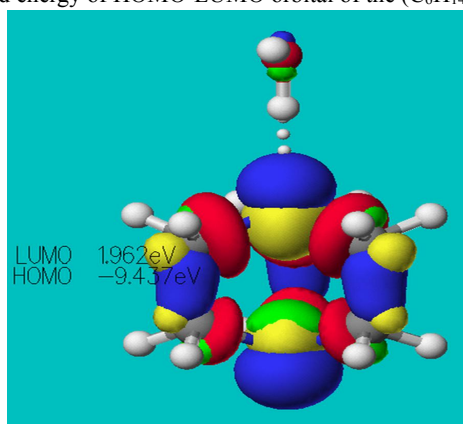
Figure 8-b: Calculated energy of HOMO-LUMO orbital of the $C_6H_{12}N_2.H_2O$ compound.
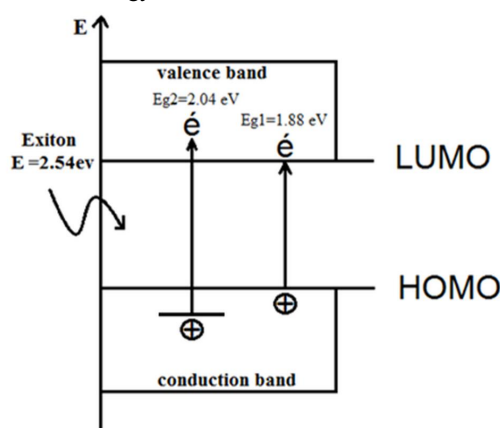
Figure 9: Explanatory diagram for the two types of transitions in $(C_6H_{14}N_2)_2[Bi_2Cl_{10}].2H_2O$.

3.5 The crystal morphology study

Significant efforts have been made in the last few decades to predict precisely the growth morphology of crystals because crystal morphology is a key element in many industrial processes like pharmaceutical, drug design[17], explosives[10], cements and has an enormous impact in the materials processing stages. The crystal morphology prediction was obtained by BFDH (Bravais-Fridel and Donnay-Harker)[18–19-20] algorithm calculation using Mercury (CSD 3.0.1)[14]. The program uses the crystal lattice parameters and the symmetry space group to generate a list of

possible growth faces and their relative growth rates. Figure 10 shows the Bravais, Friedel, Donnay and Harker (BFDH) crystal morphology based on the d_{hkl} indices and the experimental morphology of the hybrid crystals. It has found that the crystal morphology is a polyhedral shape with 16 symmetrical facets. The crystallographic planes (110), (11-1), (100), (1-1-1), (1-10), (020), (011), (01-1), (0-11), (0-1-1), (0-20), (-110), (-111), (-100), (-1-11) and (-1-10) are clearly identified.

It is observed that the growth rate of the crystal along the 'b' axis is higher than those are the 'a' and 'c'-axis. It probably explains that the growth of the hybrid crystals was done by means of association of organic- inorganic layers along the 'a' direction.
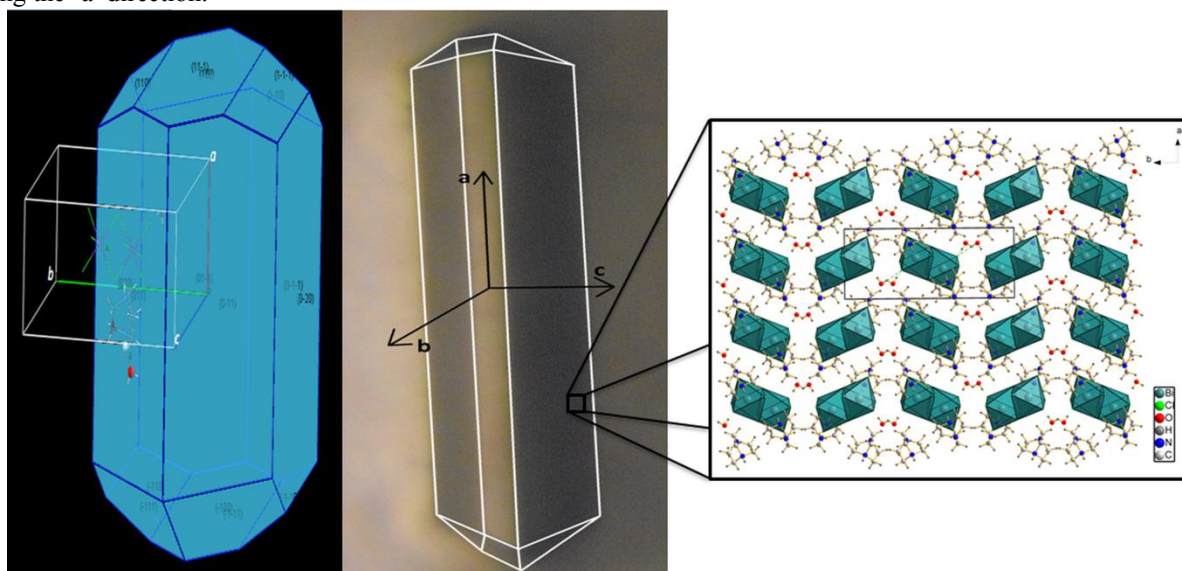
Figure 10: Predicted and real morphology of the crystals and the arrangement of the different layers in the structure.

3.6 Thermal properties (TGA, DTA, DSC)

3.6.1 Thermo-Gravimetric Analysis TGA and Differential Thermal Analysis DTA

To confirm and quantify the presence of water in the structure, Thermo-Gravimetric Analysis (TGA) coupled to Differential Thermal Analysis (DTA) were carried out. The obtained experiment diagram, shown in figure 11, reveals an endothermic phenomenon assigned to the departure of water from the structure. The dehydration, happening in a large domain between 80 and 140°C, corresponds to an observed loss of mass of $\Delta m=3.3(2)\%$. On the other hand, this proportion corresponds to the expected amount of two water molecules in the compound formula and confirms the structural investigations.

3.6.2 Differential Scanning Calorimetry (DSC)

The thermal stability of the studied crystals was investigated by Differential Scanning Calorimetry (DSC) technique. Figure (12-a) and (12-b) show the DSC diagram of the hybrid compound recorded upon heating and cooling speed of 2.5°C.min^{-1}. The scan between -45 to 250 °C reveals two types of irreversible transition happening only in heating:

* An endothermic phenomenon starting at -6.4°C (figure 12-a) and presenting an integrated enthalpy ($\Delta H_a^°$) value of 1 J.g^{-1} assigned probably, to an irreversible structural transition and to be verified by low temperature single crystal diffraction investigation.

*A strong endothermic transition (figure 12-b) takes place from 86.8 to 111.1°C. This transition has a value of integrated enthalpy ($\Delta H_b^°$) equal to 97.1 J/g assigned probably to an irreversible structural transition.

The examination of figure 12-b combined with the TGA results confirms that the endothermic transition which is the first part of the band caused by the water molecules that leaves the structure.
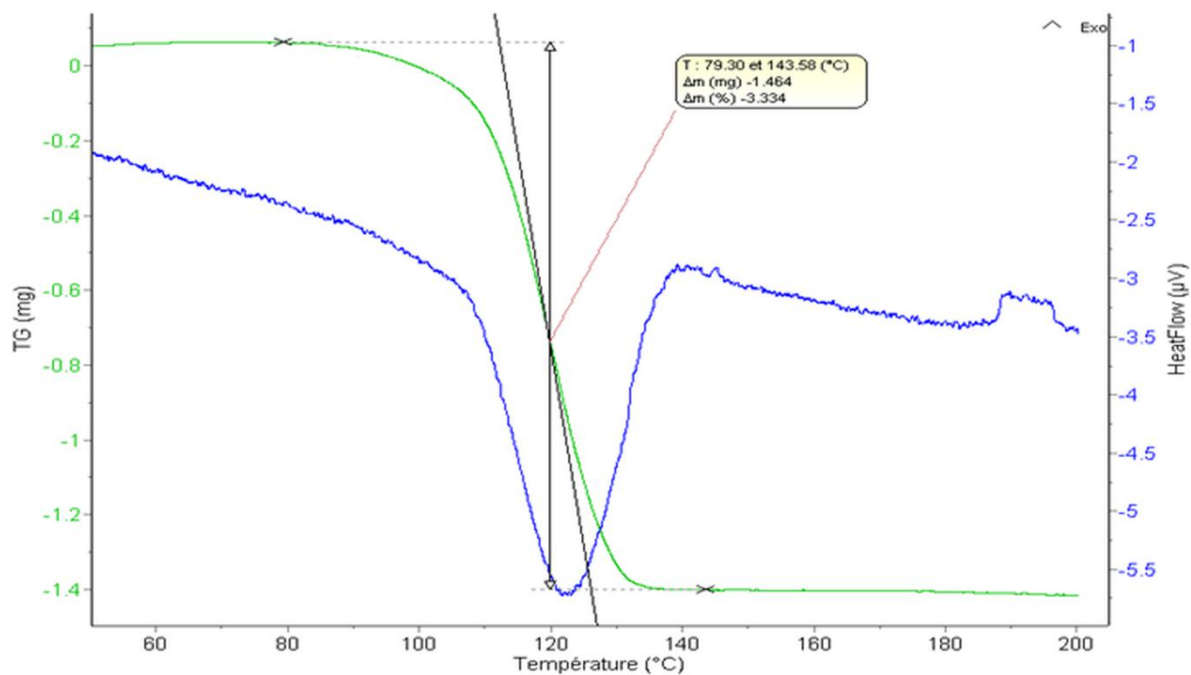
Figure 11: TGA-DTA thermogram of the studied compound.
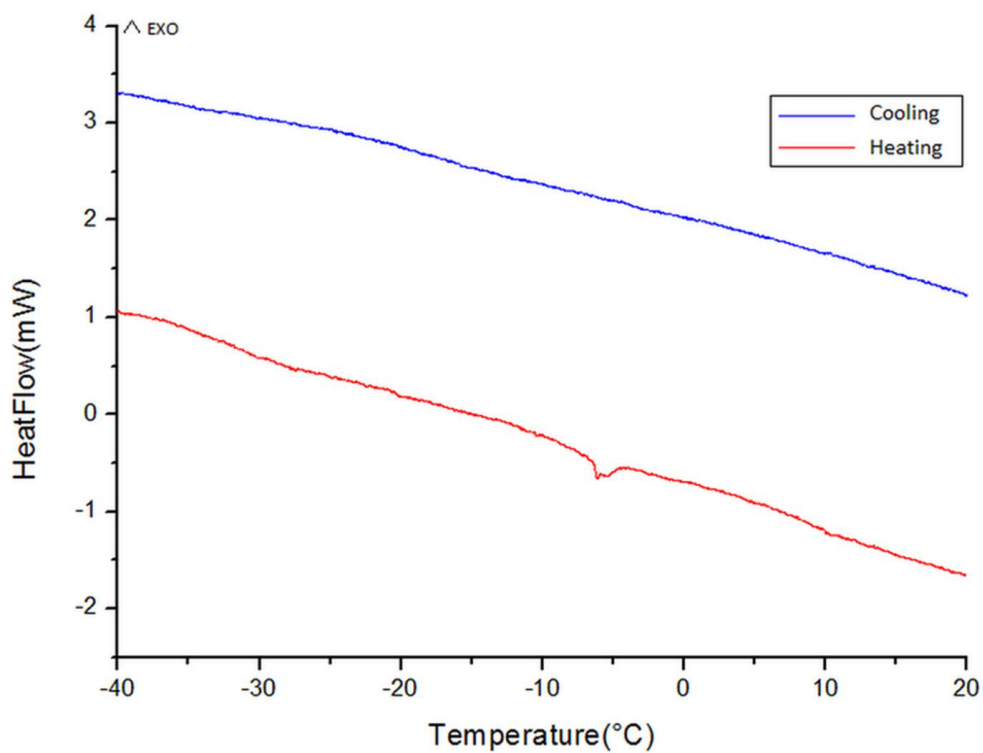
Figure 12-a: Heating/cooling thermorgram of hybrid compound in the range[-40;+20]°C.
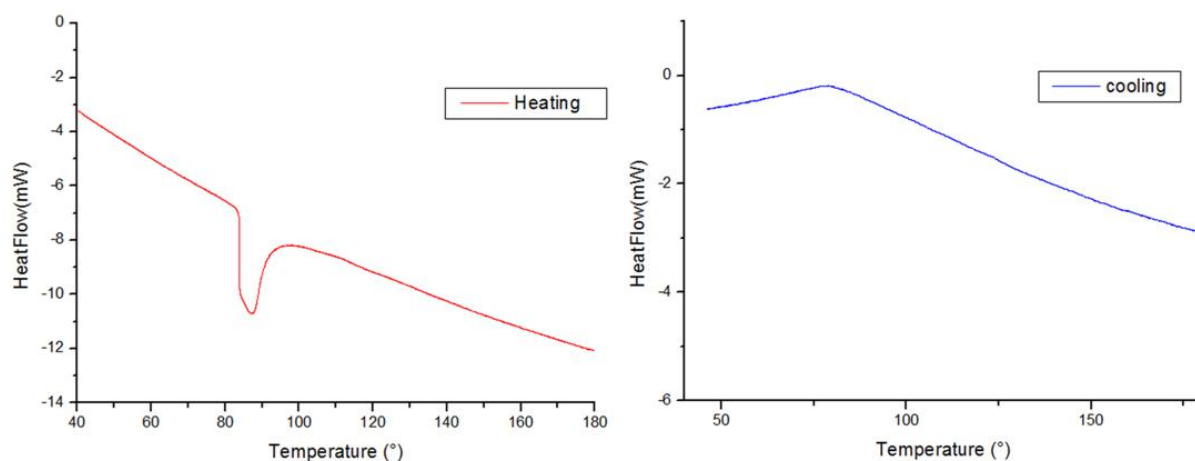
Figure 12-b: Heating/cooling thermogram of hybrid compound in the range[+40;+180]°C.

4. Conclusion:

The bis(1,4-diazabicyclo[2.2.2]octane)octachlorido-di-bismuthate(III) dihydrate is a new synthesized hybrid compound. The single crystal X-ray diffraction was used to solve and refine the structure. The X-ray powder diffraction technique was applied to control the purity of the obtained phase. This compound has been characterized by Fourier Transform Infra-Red analysis. The PM3 semi-empirical simulation combined to IR spectroscopy allow the assignment of the observed bands to the vibration frequencies. The photoluminescence experiment indicates that the compound can be ranged in the semi-conductor class with two energy gaps and could be probably used in photovoltaic application. The BFDH algorithm was used to predict the theoretical crystals morphology and makes easy the attribution of the crystallographic axis. It gives also an idea about the crystal growth directions. The differential scanning calorimetry and the thermogravimetric analysis were applied to confirm the presence of two water molecules per formula.

References

1. Jakubas R, Sobczyk L. Phase transitions in alkylammonium halogenoantimonates and bismuthates. Phase Transit. 1990; 20:163–93. https://doi.org/10.1080/01411599008206873.
2. Chaabouni S, Kamoun S, Jaud J. J Chem Crystallogr. 1998; 28:209–12. https://doi.org/10.1023/A:1022474327917.
3. Ishihara T, Takahashi J, Goto T. Optical properties due to electronic transitions in two-dimensional semiconductors $(C_nH_{2n+1}NH_3)_2PbI_4$. Phys Rev B Condens Matter. 1990; 42:11099–107. https://doi.org/10.1103/PhysRevB.42.11099
4. Lacroix PG, Clément R, Nakatani K, Zyss J, Ledoux I. Stilbazolium-MPS3 Nanocomposites with Large Second-Order Optical Nonlinearity and Permanent Magnetization. Science. 1994; 263:658–60. https://doi.org/10.1126/science.263.5147.658
5. Ahmed IA, Blachnik R, Reuter H, Anorg Z. Synthesis and Thermal Behaviour of Compounds in the System[Ph$_4$P]Cl/BiCl$_3$ and the Crystal Structures of[Ph$_4$P]$_3$[Bi$_2$Cl$_9$]·2CH$_2$Cl$_2$ and[Ph$_4$P]$_2$[Bi$_2$Cl$_8$]·2CH$_3$COCH$_3$. Allg.Chem. 2001; 627:2057. https://doi.org/10.1002/1521-3749(200109)627:93.0.CO;2-7.
6. Jakubas R, Piecha A, Pietraszko A, Bator G. Structure and ferroelectric properties of $(C_3N_2H_5)_5Bi_2Cl_{11}$. Phys Rev B Condens Matter Mater Phys. 2005; 72:104107–15. https://doi.org/10.1103/PhysRevB.72.104107.
7. Ben Rhaiem T, Boughzala H, Driss A. Bis(1,4-diazo-niabi-cyclo-[2.2.2]octa-ne) di-μ-chlorido-bis-[tetra-chlorido-anti-monate(III)] dihydrate. Acta Crystallogr Sect E Struct Rep Online. 2013; 69:m330. https://doi.org/10.1107/S160053681301307X
8. Ferjani H, Boughzala H, Driss A. Poly[bis-(1-carbamoylguanidinium)[tri-μ-chlorido-dichloridobismuthate(III)]]. Acta Crystallogr Sect E Struct Rep Online. 2012; 68:m615.https://doi.org/10.1107/S1600536812015668
9. Duisenberg AJ. Indexing in single-crystal diffractometry with an obstinate list of reflections. J Appl Cryst. 1992; 25:92–96. https://doi.org/10.1107/S0021889891010634.
10. ter Horst JH, Kramer HJ, van Rosmalen GM, Jansens PJ. Molecular modelling of the crystallization of polymorphs. Part I: the morphology of HMX polymorphs. J Cryst Growth. 2002; 237:2215–20. https://doi.org/10.1016/S0022-0248(01)02278-3.
11. Sheldrick GM. A short history of SHELX. Acta Crystallogr. 2008; A64:112–22. https://doi.org/10.1107/S0108767307043930.
12. Farrugia LJ. WinGX suite for small-molecule single-crystal crystallography. J Appl Cryst. 1999; 32:837–38.

https://doi.org/10.1107/S0021889899006020.

13. CaChe: work system Pro Version 7.5.0.85, Fujitsu Limited.2000–2006 Oxford Molecular.

14. Macrae CF, Bruno IJ, Chisholm JA, Edgington PR, McCabe P, Pidcock E, Rodriguez-Monge L, Taylor R, van de Streek J, Wood PA. Mercury CSD 2.0 – new features for the visualization and investigation of crystal structures. J Appl Cryst. 2008; 41:466–70. https://doi.org/10.1107/S0021889807067908.

15. Rietveld HM, Maslen EN, Clews CJ. An X-ray and neutron diffraction refinement of the structure of p-terphenyl. Acta Crystallogr B. 1970; 26:693–706. https://doi.org/10.1107/S0567740870003023.

16. Barczynski P, Dega-Szafran Z, Katrusiak A, Perdoch W, Szafran M. Unusual 2:3:2 complex of DABCO mono-betaine with HCl and H_2O studied by X-ray diffraction, DFT calculations and spectroscopic methods. J Mol Struct. 2009; 938:283–90. https://doi.org/10.1016/j.molstruc.2009.09.044.

17. Coombes DS, Catlow CR, Gale JD, Hardy MJ, Saunders MR. Theoretical and experimental investigations on the morphology of pharmaceutical crystals. J Pharm Sci. 2002; 91:1652–58. https://doi.org/10.1002/jps.10148

18. Bravais A. Etudes Cristallographiques. Paris: Gauthier Villars; 1866.

19. Friedel G. Bull Soc Fr Mineral. 1907; 30:326.

20. Donnay JD, Harker D. Am Mineral. 1937; 22:463.